# The effect of vortex suppression on the large-scale epitaxial growth of unidirectional $MoS_2$

Zhaofang Cheng[a, b], Kelun Deng[b], Lina Chen[b], Shijun Duan[b], Shaodan He[b], Xudong Zhang[b], Zipeng Wu[b], and Minggang Xia[a, b*]

[a] *MOE Key Laboratory for Nonequilibrium Synthesis and Modulation of Condensed Matter, School of Physics, Xi'an Jiaotong University, 710049, People's Republic of China*

[b] *Department of Applied Physics, School of Physics, Xi'an Jiaotong University, 710049, People's Republic of China*

(Some figures in this article are in color only in the electronic version.)

[*] Corresponding author. E-mail: xiamg@ mail.xjtu.edu.cn (Minggang Xia)

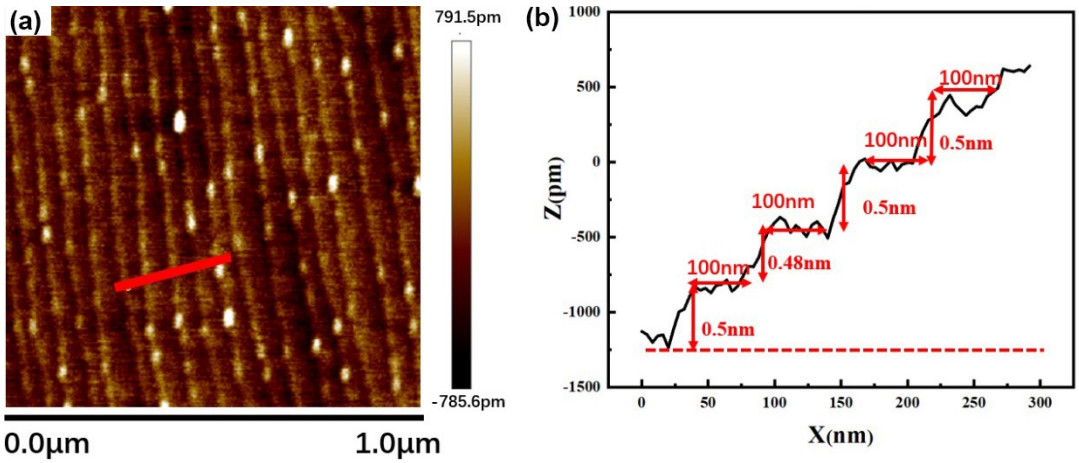


Fig. S1 AFM image of the annealed sapphire (0001) surface (a) and the height curve at the red line in (a). The surface exhibits regular, sawtooth-shaped atomic steps with an average step height of 0.5 nm and a root-mean-square (RMS) roughness of approximately 0.18 nm over a 1 μm × 1 μm area. The step edges are straight and continuous, providing periodic nucleation sites that break the energetic degeneracy of antiparallel $MoS_2$ domains.

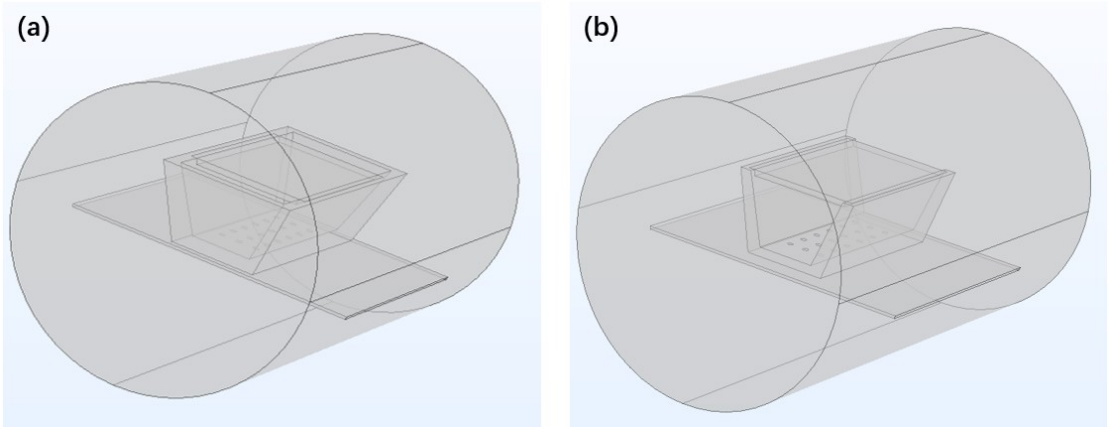


Fig. S2 COMSOL models of the two alumina boat configurations. (a) Model of the traditional enclosed boat. (b) Model of the novel open-ended boat.

1) Justification of laminar flow assumption

The Reynolds number (Re) is calculated based on the quartz tube inner diameter (D) and the bulk carrier gas velocity (u): $Re=\rho uD/\mu$, where $\rho$ is argon density and $\mu$ is dynamic viscosity. The mean velocity is $u=Q/A$, with Q is the total Ar flow rate and $A=\pi(D/2)^2$ the cross-sectional area. In this work, Q=100 sccm and D=47 mm. At room temperature ($T_0$=293 K), $\rho_0$=1.784 kg/m$^3$, $\mu_0=2.27\times10^{-5}$ Pa·s. Thus $Re_0$~3.55. At the growth temperature (T=720 °C=993 K), the dynamic viscosity is obtained from Sutherland's formula for argon: $\mu(T)=\mu_0\ (T/T_0)^{3/2}(T_0+S)/(T+S)$, where S=144 K. The density scales as $\rho=\rho_0\times(T_0/T)$, thus $Re_{993}$~0.44. Both values ($Re_0$~3.55 and $Re_{993}$~0.44) are far below 2300, confirming a strongly laminar flow regime across the entire temperature range.

2) Justification of incompressible flow assumption

The Mach number (Ma=u/c, where c is the speed of sound in argon, ~320 m/s at room temperature and ~520 m/s at 993 K in this work) is: Ma ~$1.4\times10^{-5}\ll0.3$. Therefore, density variations due to pressure changes are negligible, and the incompressible Navier–Stokes formulation is valid.

3) Buoyancy and natural convection

Natural convection arises from density gradients due to temperature differences. However, in our specific reactor geometry, buoyancy effects are effectively suppressed for two reasons: **Horizontal tube with face-down substrate**. The hot substrate is located above the $MoO_3$ source (face-down configuration). The temperature gradient is primarily vertical (hot source at bottom, cooler substrate above), which creates a stable density stratification (lighter hot gas below heavier cool gas). **Confined narrow gap**. The distance between the $MoO_3$ source and the substrate is only ~10 mm. In such a shallow horizontal cavity with heating from below and cooling from above, buoyancy effects are effectively suppressed.

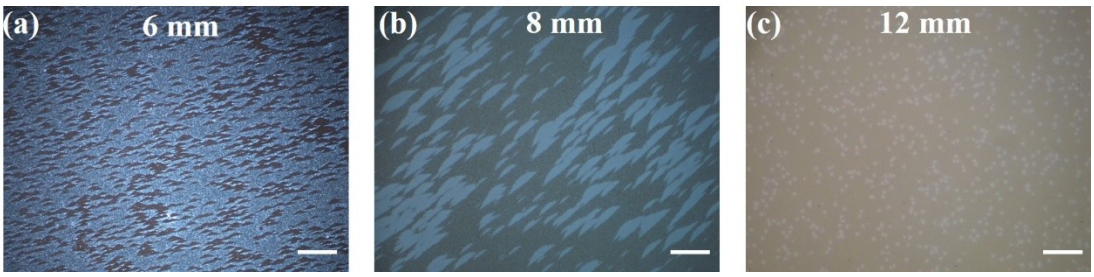


Fig. S3 Effect of substrate–precursor gap on $MoS_2$ growth. (a-b) Gap < 10 mm (6–8 mm): excessive nucleation and multilayer formation due to high $MoO_3$ concentration. (c) Gap > 10 mm (12 mm): incomplete coverage and small domains due to insufficient precursor flux. The optimal gap of 10 mm (used in this work) provides a balance between adequate precursor supply and controlled nucleation. Scale bar: 10 μm.

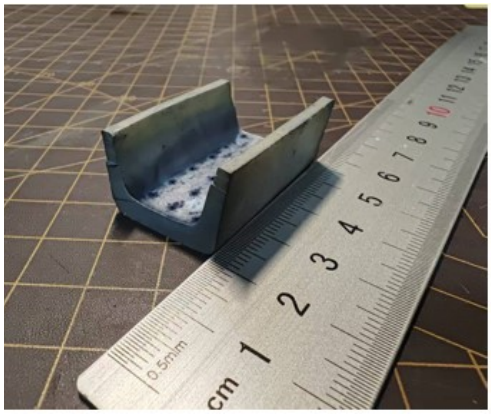

Fig. S4 The photograph of alumina crucible. The boat has an outer length of 45 mm, outer width of 22 mm, and outer height of 15 mm, with both ends fully open to allow axial gas flow through the boat. During CVD growth, 1 mg of $MoO_3$ powder was dispersed in a 3×6 array across an alumina crucible.

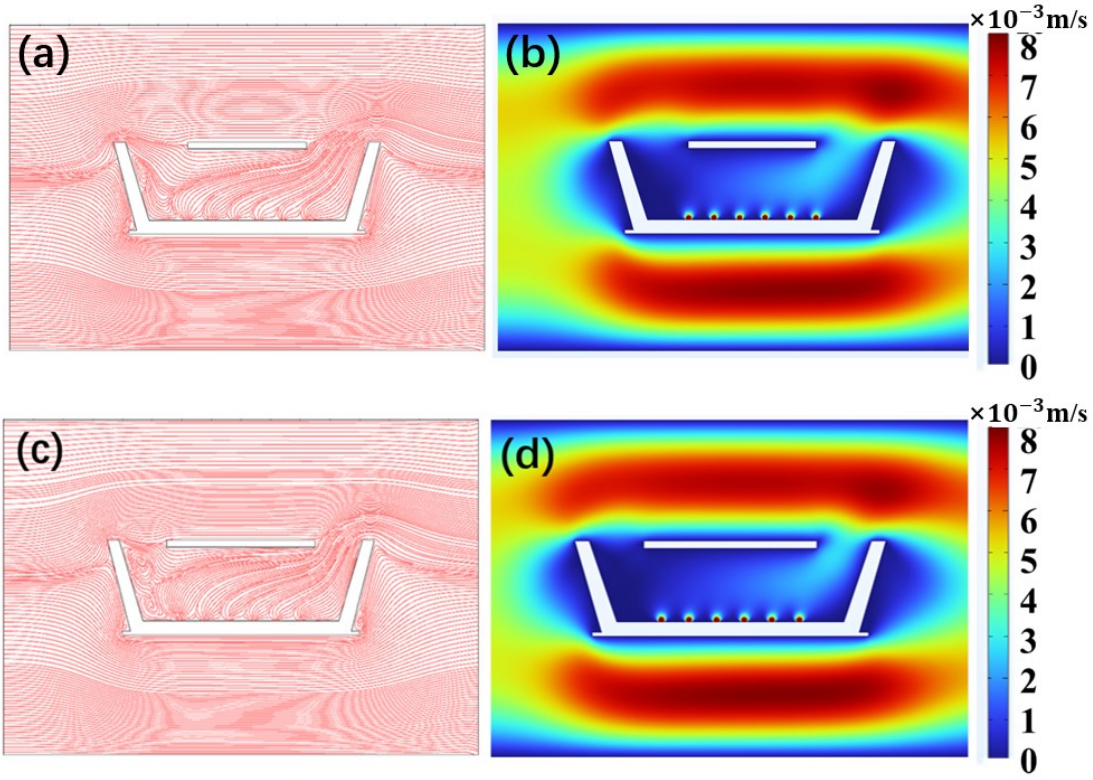


Fig. S5 COMSOL simulation of the traditional enclosed alumina boat with varying substrate sizes. (a) Flow field and (b) velocity magnitude for a 1-inch substrate, respectively; (c) flow field and (d) velocity magnitude for a 1.5-inch substrate, respectively.

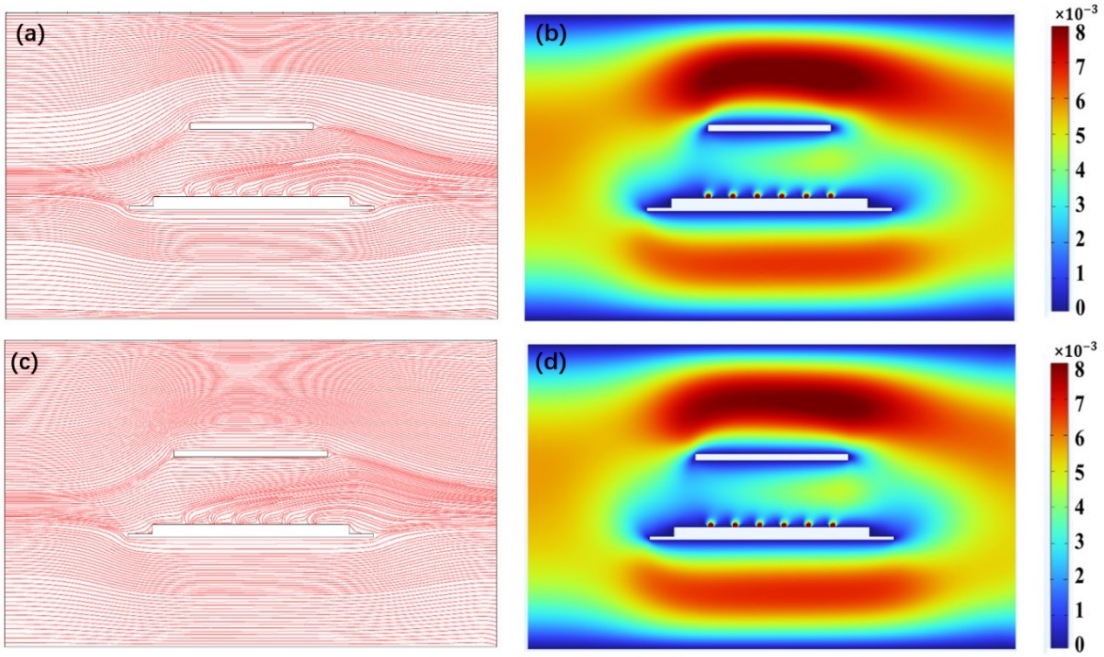


Fig. S6 COMSOL simulation of the open-ended alumina boat with varying substrate sizes. (a) Flow field and (b) velocity distribution for a 1-inch substrate. (c) Flow field and (d) velocity distribution for a 1.5-inch substrate.

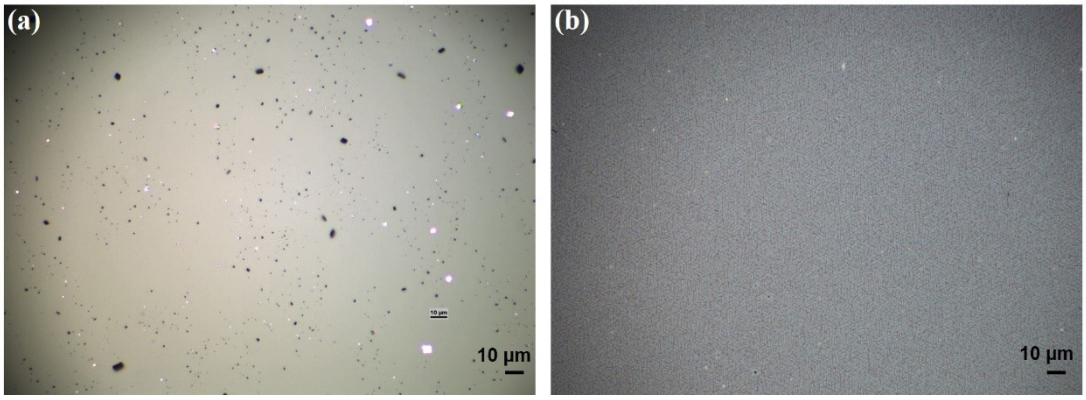


Fig. S7 Experimental validation of CFD predictions using $MoO_3$ deposition as a flow tracer. Control growth experiments were performed without sulfur under otherwise identical conditions. (a) In the closed boat, $MoO_3$ deposition is highly non-uniform: sparse coverage near the front edge (where the vortex is predicted). (b) In the open-ended boat, $MoO_3$ deposition is uniform across the entire substrate surface. The contrast qualitatively confirms that the open-ended boat eliminates the vortex and establishes uniform precursor delivery, consistent with the CFD simulations.

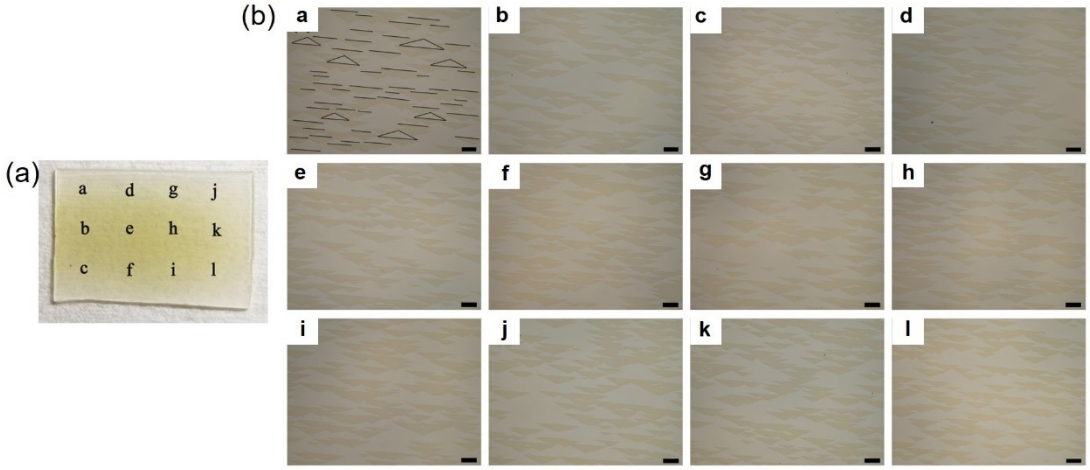


Fig. S8 Uniform unidirectional alignment of $MoS_2$ domains across a large-area substrate. (a) Photograph of $MoS_2$ grown on 1.5-inch c-sapphire substrate for 5 min. The slight color variation across the wafer arises from minor local differences in the substrate–precursor distance caused by dimensional tolerances during substrate cutting, which can lead to local variations in domain size or thickness of $MoS_2$. (b) Optical microscopy images of $MoS_2$ islands at 12 different spots marked in (a). The optical images at different positions show unidirectional orientation of the $MoS_2$ grains. The scale bars for (a-i) are 25 μm.

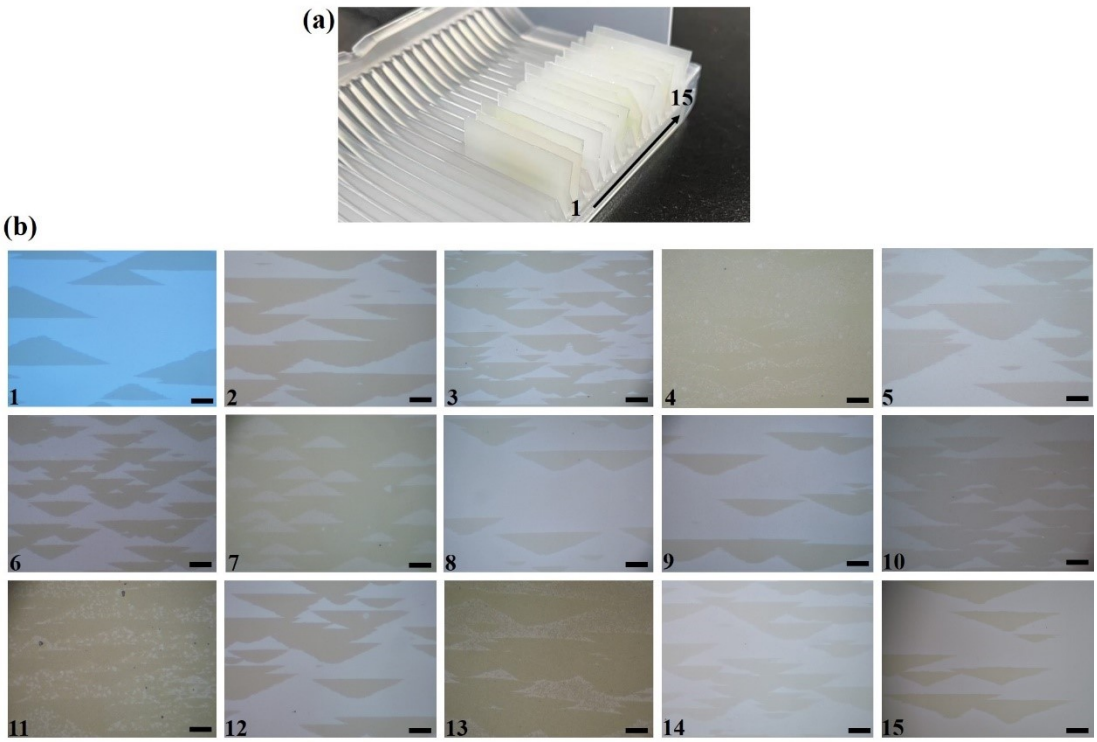


Fig. S9 Growth reproducibility and yield statistics for the open-ended boat configuration. (a) Yield of continuous monolayer $MoS_2$ films over 15 consecutive growth runs under identical conditions. (b) Orientation uniformity for early-stage growth (5 min). Optical images from random positions across 15 representative runs were analyzed; 12 out of 15 runs (≈80%) produced uniform monolayer films across the entire 1.5-inch wafer, and the fraction of unidirectionally aligned triangular domains was consistently above 99% in all runs, demonstrating excellent reproducibility of epitaxial alignment. Scale bar, 10 μm.

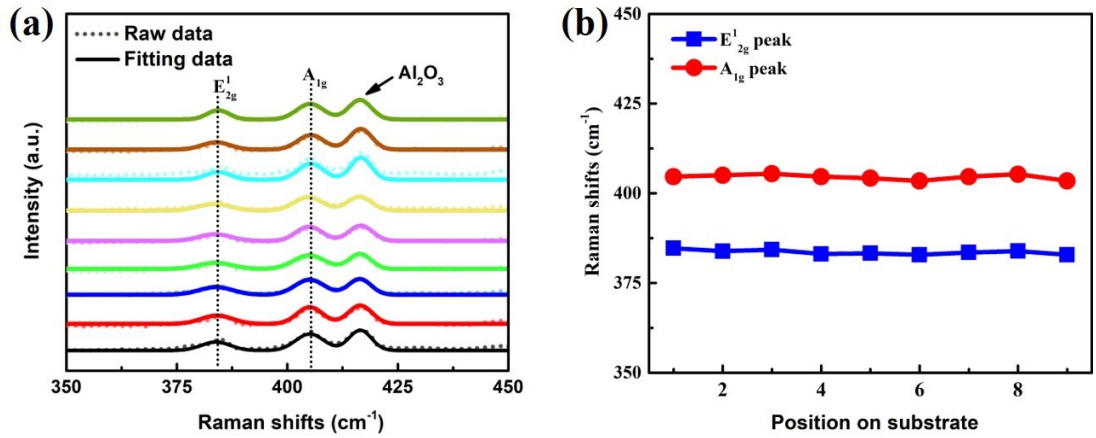


Fig. S10 (a) The Raman spectra were acquired from nine uniformly scattered sample spots over $MoS_2$ film. (b) The specific data of $E^1_{2g}$ and $A_{1g}$ peaks corresponding to nine Raman spectra showed in (a).

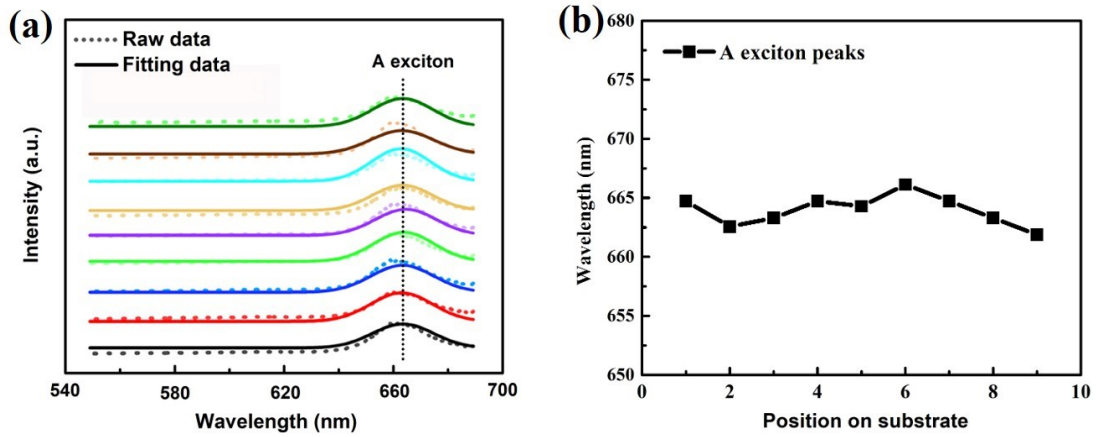


Fig. S11 (a) The PL spectra were acquired from nine uniformly scattered sample spots over $MoS_2$ film. (b) The specific data of A exciton peaks corresponding to nine PL spectra showed in (a).

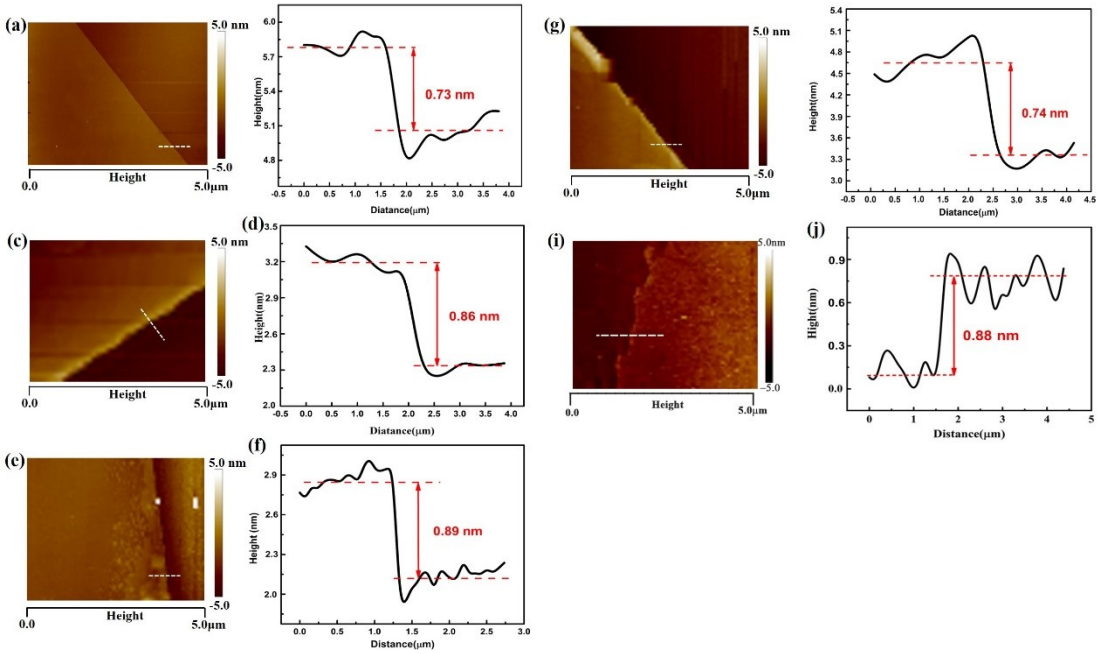


Fig. S12 AFM line profiles from five random positions on the 1.5-inch sapphire wafer after $MoS_2$ growth. The measured thickness values range from 0.73 nm to 0.89 nm, with an average of 0.81 nm and a standard deviation of ±0.08 nm, all consistent with monolayer $MoS_2$.